Article:
Wu, D, Li, J, Song, D et al. (3 more authors) (2023) Development of a Novel Ball-and-Socket Flexible Manipulator for Minimally Invasive Flexible Surgery. IEEE Transactions on Medical Robotics and Bionics, 5 (2). pp. 278-288. ISSN 2576-3202

https://doi.org/10.1109/tmrb.2023.3265714

Development of a Novel Ball-and-Socket Flexible Manipulator for Minimally Invasive Flexible Surgery

Di Wu, Jichen Li, Dezhi Song, Zhiqiang Zhang, Kaifeng Wang, Chaoyang Shi

***Abstract*—This work proposes a novel flexible manipulator consisting of a series of 2-DOF vertebrae based on a ball-and-socket joint that is connected by a ball-shaped surface and a cup-shaped socket and constrained by pins for circumferential rotation. This manipulator can demonstrate outstanding torsional stiffness since the circumferential rotation between the vertebrae is constrained by four ball pins. The point contact between ball pins and guideways effectively reduces the friction between the vertebrae, thus allowing the designed manipulator to yield a smooth bending shape with constant curvature. This manipulator features high axial and torsional stiffness, excellent bending performance, sufficient loading capacity, and convenient integration with surgical instruments. Moreover, the excellent torsional stiffness enables this manipulator to efficiently transfer torque and be applied in in-situ torsional motion, effectively addressing the typical issue of limited dexterity for torsional motion. The kinematic modeling of the proposed manipulator under in-situ torsional motion has been derived, and its workspace has been analyzed. A robotic system has been assembled, and experiments have verified the proposed design and modeling validity. The results show that the maximum position errors in bending motion are 2.39% (horizontal direction) and 1.98% (vertical direction), and its torsional stiffness is 21.13N·mm/deg, which is 46 times higher than that of a typical spherical flexible manipulator (SFM). Such merits support this manipulator excellently performing the in-situ torsional motion with a maximum average position error of 3.58%. Furthermore, a phantom test of the larynx has been performed to verify the potential of clinical feasibility.**

***Index Terms*— Minimally invasive flexible surgery, flexible endoscopy, flexible manipulator, in-situ torsional motion.**

I. Introduction

The robot-assisted flexible endoscopy (FE) and natural orifice transluminal endoscopic surgery (NOTES) are two emerging procedures for minimally invasive flexible surgery (MIFS), offering advantages in terms of non-incision or non-visible-scar procedures, fewer damages, faster postoperative recovery, and fewer complications [1,2]. The MIFS utilizes a flexible manipulator instead of the straight and rigid manipulator in minimally invasive surgery (MIS) to pass through a natural cavity or small incisions for diagnosis and treatment. Flexible manipulators have been increasingly developed and play an essential role in the MIFS [3]. Compared with traditional rigid instruments, flexible manipulators feature high dexterity and an extensive workspace to perform complex examinations and surgical operations through narrow cavities or paths and provide relatively safe physical interactions that significantly reduce tissue damage and accelerate the postoperative recovery of patients [4–6]. The distal end of flexible manipulators is typically required to integrate various surgical tools to approach the lesion for further examinations and treatments during surgical procedures. Therefore, flexible manipulators are required to feature sufficient payload to provide adequate interaction forces and maintain stability under external loading [7]. However, there is a dilemma between high dexterity and high payload, which needs to be balanced effectively [8,9]. In addition, surgeons typically need to rotate the manipulator to adjust the attitude of surgical tools when performing surgical operations such as endoscopic exploration, drilling, and suturing. Nonetheless, the dexterity of flexible manipulators is typically limited in terms of torsional motion. In-situ torsional motion supports the manipulator to be rotated while keeping the distal direction unchanged, which can effectively improve the dexterity of the manipulator [10,11]. However, in-situ torsional motion requires high torsional stiffness for the flexible manipulators to transmit torque, which is challenging for the design of flexible manipulators. Therefore, developing flexible manipulators with high dexterity, high torsional stiffness, and high loading capacity is significant and has attracted considerable attention and investigation.

Flexible manipulators based on discrete-style vertebrae have been widely researched. They are commonly composed of a series of rigid vertebrae based on mechanical joints [12], such as rolling joints [13–15], gear-driven joints [16], and sliding joints [17–19], and can be bent in a plane or space by driving cables. Payne et al. [20] proposed a 1-DOF flexible manipulator consisting of stacked vertebrae based on rolling joints and integrated four Nitinol rods to provide a compliant elastic backbone for arthroscopy and orthopedic procedures. This design achieved a large bending range of ±170° and an external loading force of 3N. However, it lacked the lateral anti-interference capacity to prevent the vertebrae from slipping, resulting in poor connection stability and inaccurate control. To overcome such limitations, the typical spherical flexible

Mannuscript received Jan 11, 2023. This work is supported in part by National Natural Science Foundation of China under Grant 92148201, Grant 51721003, Grant 62211530111, Grant 61973231, and Royal Society under IEC\NSFC\211360. D. Wu and J. Li contribute equally to this work. Corresponding author: K. Wang and C. Shi.

D. Wu , J. Li, D. Song, K. Wang and C. Shi are with Key Laboratory of Mechanism Theory and Equipment Design of Ministry of Education, School of Mechanical Engineering, Tianjin University, Tianjin, 300072, China. Z. Zhang is with School of Electronic and Electrical Engineering, University of Leeds, Leeds, LS2 9JT, UK. This work is also supported by International Institute for Innovative Design and Intelligent Manufacturing of Tianjin University in Zhejiang, Shaoxing 312000, CN.

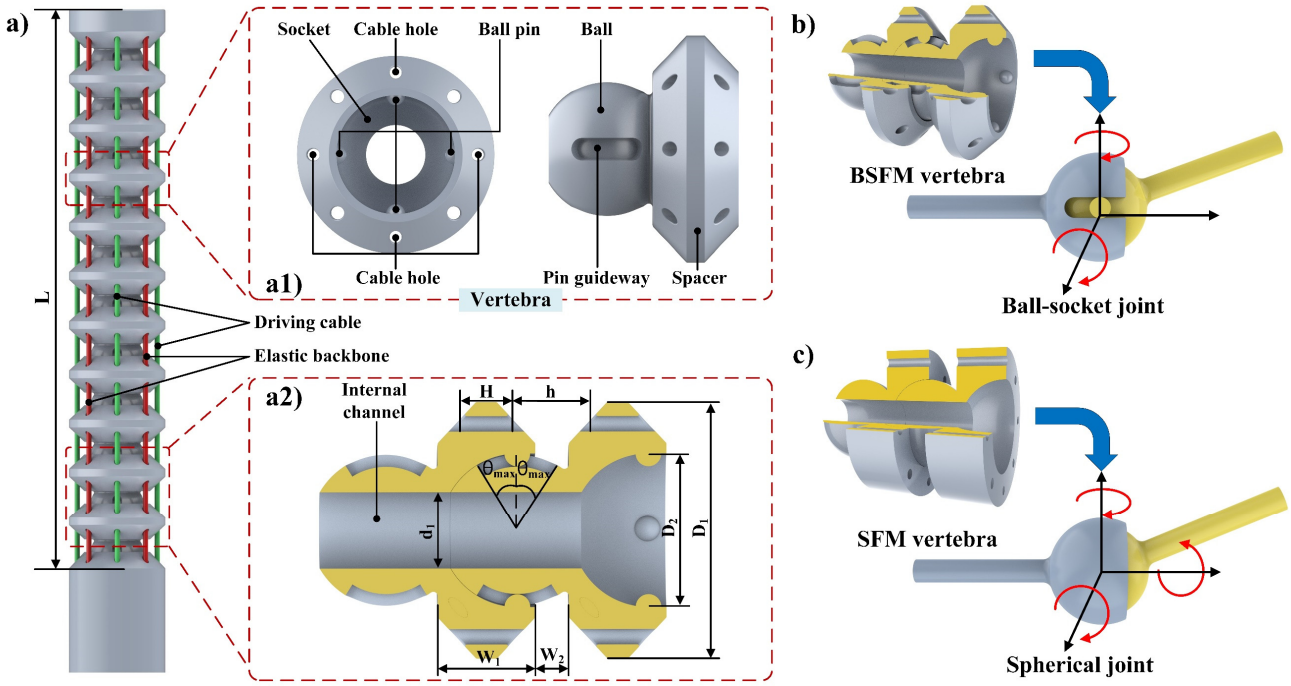

Fig. 1. Overview of the ball-and-socket flexible manipulator (BSFM). a) Detailed structure design of the BSFM manipulator. b) Schematic diagram of the BSFM vertebra. c) Schematic diagram of the traditional SFM vertebra.

manipulators (SFM) that consist of a serial chain of vertebrae are proposed as discrete-style flexible structures to generate bending motions with high stability and dexterity. These vertebrae are inspired and designed based on the traditional 3-DOF spherical joint whose structure is connected by a spherical surface and a cup-shaped socket. Li et al. [21,22] proposed a 2-DOF constrained cable-driven SFM manipulator based on the spherical joints to achieve stable connections and a large bending angle of 180°. However, this design exhibited high frictional nonlinearity due to the extensive spherical contact of the vertebrae, leading to poor constant curvature characteristics and reduced loading capacity. Hong et al. [23] further developed this SFM manipulator by embedding two Nitinol tubes in the body to enhance its loading capacity for maxillary sinus surgery, but this design reduced one bending DOF. This design can be bent up to 270° to reach the target position flexibly and withstand a payload of 1.5N. However, high friction remains between vertebrae, leading to non-constant curvature in large bending deformation. In addition, the above-mentioned designs lack focus on the anti-torsion capacity which is challenging for the lengthy discrete manipulators' design [24]. The flexible manipulators struggle to transfer torque efficiently when torsional stiffness is insufficient, yielding significant inconsistencies between the proximal and distal ends of the manipulator and a decrease in the in-situ torsional motion accuracy. To improve the torsional stiffness of flexible manipulators, Kim et al. [25] proposed a discrete manipulator consisting of protrusion-based vertebrae which constrain the lateral sliding and torsional motion between the vertebrae by the matching of guideways and protrusions. However, the bending performance is unfavorable with an average position error of 4.59%. Kong et al. [10] designed a 2-DOF manipulator based on an array of orthogonal arrangements of sliding joints and improved its torsional stiffness through the cooperation of protrusions and grooves. This design was applied to the in-situ torsional motion to improve its dexterity and workspace. However, the torsional stiffness of this design was insufficient, affecting the torque transfer efficiency and the accuracy of the in-situ torsional motion with a maximum average positioning error of 5.75%. Therefore, discrete manipulators usually demonstrate poor constant curvature performance due to high and uneven friction, resulting in failing to accurately fit curves with continuous tangential vectors [6,26], and tend to shrink into a zigzag shape for the initial stage due to static instability [27]. In addition, such manipulators typically suffer from poor torsional stiffness, leading to difficulties in anti-torsion and effective torque transmission, and thus fail to be applied in in-situ torsional motion to address the typical issue of limited dexterity for torsional motion.

To overcome these limitations, this work proposes a novel ball-and-socket flexible manipulator (BSFM), which is composed of a series of vertebrae based on a ball-and-socket joint structure and driven by two pairs of antagonistic cables. The presented manipulator features advantages such as high dexterity with constant curvature characteristics, outstanding torsional stiffness, and sufficient loading capacity, allowing this design effectively transfer torque and be applied in the in-situ torsional motion to overcome the limitation of insufficient dexterity of flexible manipulators in torsional motion. The kinematic model and workspace of the BSFM manipulator under in-situ torsional motion have been established and analyzed. Meanwhile, the performance validation experiments and a phantom test have been conducted to verify its performance and potential for clinical feasibility in MIFS.

II. Materials and Methods

A. Design Overview

A novel BSFM flexible manipulator that consists of a chain of vertebrae has been inspired by a ball-and-socket joint and the detailed design is illustrated in Fig. 1a). The ball-and-socket joint is typically formed by a ball-shaped surface and a cup-shaped socket and capable of generating motion around two perpendicular axes with its circumferential rotation constrained by pins, as displayed in Fig. 1b). Compared with conventional spherical joints (Fig. 1c)), the ball-and-socket joint can further effectively improve the anti-torsion capacity and transmit torque by constraining its circumferential rotation while maintaining high dexterity and connection stability. The vertebra is inspired and designed based on the improvements on the ball-and-socket joint in a small size, consisting of a socket, a ball, and a spacer, as shown in Fig. 1a1)-a2). The socket part comprises a semi-spherical hollow center and four embedded ball pins with a uniform distribution of 90°. The ball-shaped part is made of four-pin guideways and an internal channel. The spacer part is designed in a trapezoidal shape with four through-holes for cables, and four through-holes for Nitinol rods. The four pins are restricted to slide inside the guideways of the connecting vertebra to constrain the circumferential rotation and the maximum bending angle $\theta_{\max}$ of the vertebra is constrained by the length of the guideway, thus allowing $\theta_{\max}$ to be adjusted by changing the length of the guideway. Meanwhile, the point contact between the ball pins and the guideways replaced the traditional spherical contact, significantly reducing the friction between the vertebrae. The multiple vertebrae are connected by four cables to form the BSFM manipulator with 2 bending DOFs, as illustrated in Fig. 1a). Each DOF is realized by driving a pair of antagonistic cables, which go through the cable holes and are fastened to the distal end of the BSFM manipulator. Four Nitinol rods (OD=0.8 mm) are arranged around the BSFM manipulator as the elastic backbone to play the role of support and rebound. In addition, the BSFM manipulator retains a large internal channel, allowing the integration of surgical instruments such as grippers and endoscopes to facilitate examination and treatment.

Compared with other flexible manipulators, this manipulator features several significant advantages to effectively meet the needs of the MIFS. Firstly, the ball-and-socket connection enables the manipulator to maintain excellent connection stability and axial stiffness, avoiding the slip of vertebrae when the manipulator is stressed. Secondly, the stress can be evenly distributed to each vertebra with smooth bending curvature when the BSFM manipulator is bent due to the reduction of inter-vertebrae friction. Therefore, the assumption of constant curvature can be successfully applied in kinematic modeling to improve the control accuracy of the BSFM manipulator. Meanwhile, the trapezoidal spacer can minimize the gap distance of the vertebrae while ensuring the required bending angle, further improving the constant curvature performance and expanding the bending range. In addition, the torsional stiffness is significantly increased since the circumferential rotation between the vertebrae is constrained by ball pins, empowering this design to effectively prevent twisting and transfer torque. Notably, the excellent torsional stiffness also enables the BSFM manipulator to be effectively applied in in-situ torsional motion to address the difficulty of limited dexterity of manipulators in torsional motion. Finally, the BSFM manipulator also has an excellent loading capacity and static stability due to the tight vertebra connection and the arrangement of Nitinol rods as elastic backbones. Therefore, the BSFM manipulator offers high stability and dexterity, outstanding torsional stiffness, and sufficient loading capacity, providing a favorable trade-off between dexterity and stiffness.

The flexible manipulator is manufactured using the 3D-printing of stereo lithography appearance (SLA), which can achieve a 200μm accuracy and is suitable for producing complex and small structures. The manufacturing material is photosensitive resin, whose tensile and flexural modulus values are 2559MPa and 2670MPa respectively. The design parameters of the BSFM manipulator can be found in Table I.

TABLE I
Design Parameters of the Presented BSFM Manipulator

Symbol	Description	Values
L	Effective bending length of the BSFM	92mm
N	Number of the BSFM vertebrae	12
W_1	Width of the spacer	5.7mm
W_2	Gap distance between the spacers	1.97mm
H	Length of the cable hole	3.52mm
h	Gap distance between the cable hole	4.15mm
d_1	Diameter of the internal channel	4.5mm
D_1	Outer diameter of the BSFM vertebrae	15mm
D_2	Diameter of the socket of the BSFM	9mm
θ	Bending angle of each vertebra	±22°

B. Kinematic Modeling

The designed BSFM manipulator has 2 bending DOFs and 1 rotation DOF and supports the in-situ torsional motion. Its kinematic model under in-situ torsional motion has been analyzed for control as below.

1) Mapping Between Joint Space and Task Space

Three frames are established to describe the kinematic relationship between joint space and task space, as shown in Fig. 2a).

- World frame $\{W\} = \{X_W, Y_W, Z_W\}$ is fixed to the base of the manipulator, whose $X_W Y_W$ plane is parallel to the upper surface of the base vertebra and the X_W axis overlaps with the central axis of the base vertebra.
- Base frame $\{B\} = \{X_B, Y_B, Z_B\}$ is attached to the base vertebra of the BSFM, and the $X_B Y_B$ plane is defined following the plane where the centers of the ball pins of the base vertebra are located. The X_B axis points from the center of the base vertebra to the first driving cable and has an angle α with the X_W axis.
- End frame $\{E\} = \{X_E, Y_E, Z_E\}$ is attached to the distal end of the flexible manipulator. The Z_E axis is the central axis of the end joint and the X_E axis points to the direction of the first driving cable.

In addition, M_1 represents the transmission length from the

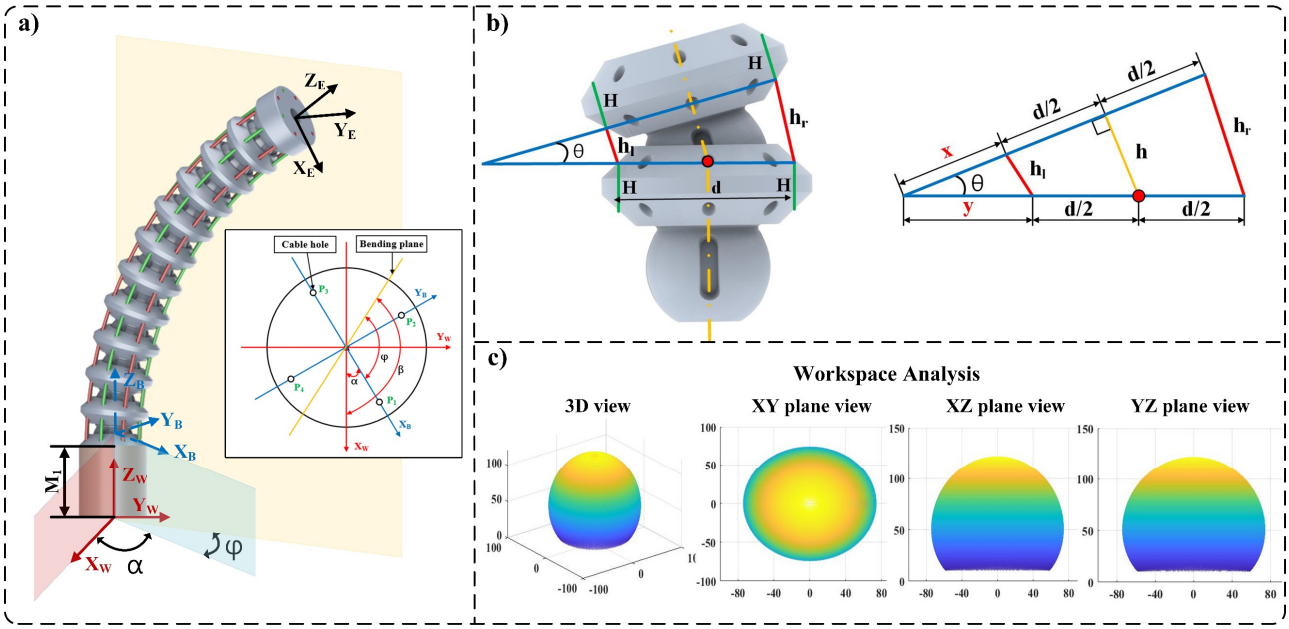

Fig. 2. Kinematic modeling and analysis of the BSFM manipulator. a) Frame definition. b) Geometric relationships between the cable length and bending angle. c) Workspace analysis of the BSFM manipulator.

base frame $\{B\}$ to the world frame $\{W\}$, and φ is the angle between the bending plane and the X_B axis. Then a homogeneous transformation matrix ${}^{W}_{E}T$ of the BSFM from the world frame $\{W\}$ to the end frame $\{E\}$ can be expressed as follows:

$$ {}^{W}_{E}T = {}^{W}_{B}T\,{}^{B}_{E}T = \begin{bmatrix} {}^{B}_{E}R & {}^{B}_{E}P_{O_E} \\ 0_{1\times3} & 1 \end{bmatrix} = \begin{bmatrix} n_x & o_x & a_x & p_x \\ n_y & o_y & a_y & p_y \\ n_z & o_z & a_z & p_z \\ 0 & 0 & 0 & 1 \end{bmatrix} \quad (1) $$

$$ {}^{W}_{B}T = rot(Z_w, \alpha) \times trans(Z_w, M_1) \quad (2) $$

Geometric analysis is adopted for the kinematic model. Since the backbone is located in the neutral plane, its length remains constant during the bending process and each vertebra can be simplified as a straight line with length $H + h$ (H is the length of the cable hole, and h denotes the pitch of the cable holes of the two adjacent vertebrae.). Assuming the same bending angle of θ for each vertebra, then the homogeneous transformation matrix can be obtained as follows:

$$ {}^{B}_{E}T = \begin{bmatrix} {}^{B}_{E}R & {}^{B}_{E}P_{O_E} \\ 0_{1\times3} & 1 \end{bmatrix} \quad (3) $$

where

$$ {}^{B}_{E}R = rot(Z_B, \varphi) \times rot(Y_B, \Theta) \times rot(Z_B, -\varphi) \quad (4) $$

$$ \Theta = N \cdot \theta \quad (5) $$

$$ {}^{B}_{E}P_{O_E} = \begin{bmatrix} p_x \\ p_y \\ p_z \end{bmatrix} = \begin{bmatrix} (H+h)\sum_{i=1}^{N} \sin(i\cdot\theta)\cos(\varphi) \\ (H+h)\sum_{i=1}^{N} \sin(i\cdot\theta)\sin(\varphi) \\ (H+h)\sum_{i=1}^{N} \cos(i\cdot\theta) \end{bmatrix} \quad (6) $$

where Θ represents the bending angle of the BSFM manipulator and N is the number of vertebrae. Based on the above equations, the inverse kinematic equations for this mapping can be calculated as:

$$ \begin{aligned} \Theta &= \cos^{-1} a_z \\ \varphi &= \tan^{-1}\left(\frac{o_z}{n_z}\right) \\ \alpha &= \cos^{-1}\left(\frac{n_x + o_y}{(1+a_z)^2}\right) \end{aligned} \quad (7) $$

2) Mapping Between Joint Space and Actuation Space

For the two adjacent vertebrae, the geometric relationship between the driving cables' length and the vertebra's bending angle is shown in Fig. 2b). The red dot represents the center of rotation of the vertebra (the center of the ball of the vertebra), which is at the same level as the upper part of the cable hole. The relationship between the cable length and the bending angle between the vertebrae is determined:

$$ h_{r/l} = \sqrt{h^2 + d^2\sin^2\left(\frac{\theta}{2}\right) \pm dh\sin\theta} \quad (8) $$

The length of the cables for the entire mechanism can be expressed below:

$$ L_{r/l} = N \cdot \left(H + h_{r/l}\right) \quad (9) $$

Thus, when the BSFM manipulator bends to any direction in space (bending direction is φ) by an angle Θ, the mapping of the BSFM from the joint space to the actuator space can be obtained as follows:

$$ L_i = N\cdot H + N\sqrt{h^2 + m^2\sin^2\left(\frac{\theta}{2}\right) + mh\sin\theta} \quad (10) $$

where $m = d \cdot \sin\left(\frac{\pi}{2}i - \varphi\right)$, $i = 1,2,3,4$. According to Eq. (10), the inverse kinematic equations between the joint space and the actuator space can be obtained as follows:

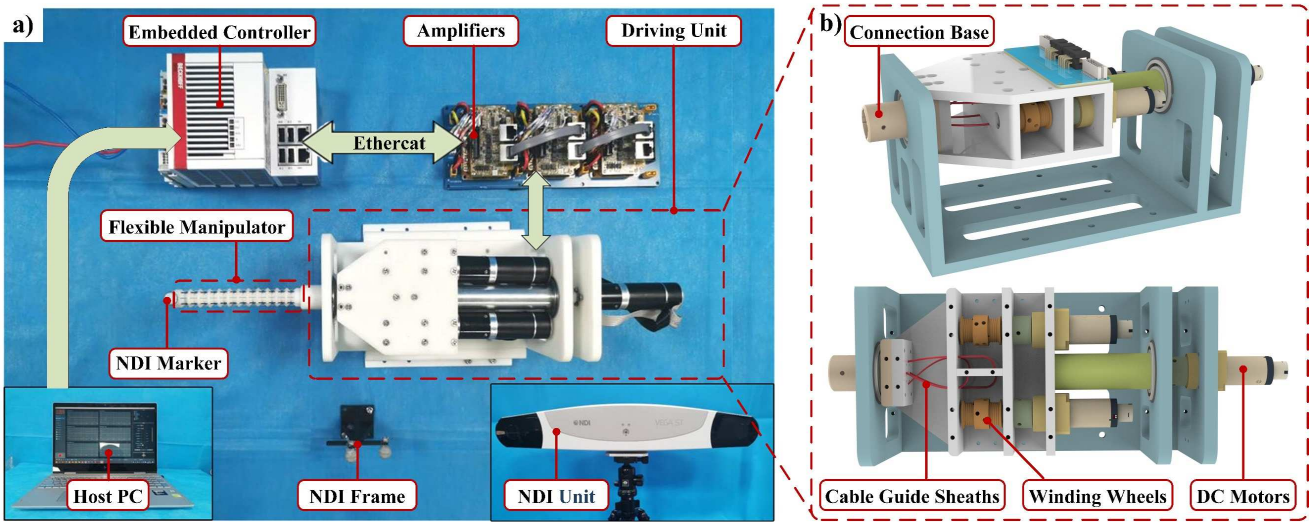

Fig. 3. a) Experimental configuration for performance investigation of the proposed flexible manipulator. b) 3D mechanical structure of the driving unit.

$$\varphi = \tan^{-1}\left(\frac{S_2^2 - S_4^2}{S_1^2 - S_3^2}\right)$$
$$\Theta = N \cdot \theta = N \cdot \sin^{-1}\left(\frac{\sqrt{(S_1^2 - S_3^2)^2 + (S_2^2 - S_4^2)^2}}{2N^2 dh}\right) \quad (11)$$

where $S_i = L_i - N \cdot H, i = 1,2,3,4$.

3) In-situ Torsional Motion

When the robot performs in-situ torsional motion, the angles β and Θ need to be kept constant, and the rotational angle α and the length of the driving cables change accordingly, as shown in Fig. 2a). Assuming that the angle of the in-situ torsion is $\Delta\alpha$, then

$$\Delta\varphi = \Delta\beta - \Delta\alpha = -\Delta\alpha \quad (12)$$

According to Eqs. (10) and (12), the length change of the cables can be calculated as follows:

$$\Delta L_i = L_i(\varphi - \Delta\alpha) - L_i(\varphi) \quad (13)$$

where $i = 1, 2, 3, 4$. In particular, the mechanism performs a pure rotational motion when only the angle α is changed.

C. Workspace Analysis

To further explore the performance of the BSFM, its workspace is analyzed using MATLAB based on the above-derived kinematic model. The basic parameters of the BSFM are assumed to be $M_1 = 20\text{mm}, \alpha \in [0,2\pi], \varphi \in [0,2\pi]$ and $\Theta \in [0,2\pi]$, and the analysis results are shown in Fig. 2c). It can be seen that the workspace forms a $112\text{mm} \times 112\text{mm} \times 75\text{mm}$ ellipsoidal surface.

III. Experiments and Results

A. Experimental Setup

The experimental configuration for performance evaluation has been illustrated in Fig. 3. This setup mainly consists of a motion control unit, a driving unit, an optical tracking unit, a prototyped flexible manipulator, and a host PC. The driving unit utilizes three DC motors (EC2232L, Vishan, China) equipped with amplifiers (Uservo-Flex, MotionG, China) to control the bending and rotational motions of the BSFM manipulator respectively. The control unit employs an embedded controller (CX-5140, Beckhoff, Germany), sends commands to amplifiers via the Ethercat bus connection, and then drives the motors via the semi-closed-loop control mode. The control frequency is set to 1kHz to ensure real-time operation. The host PC sends the desired commands to the controller and receives feedback via the ADS-based communication approach. The optical tracking unit (Polaris Spectra, NDI, Canada) is used to collect the distal position of the BSFM manipulator.

B. Investigation of the Kinematic Performances

1) Kinematic Performances of the 2-DOF Bending

The BSFM manipulator was driven to bend from -150° to 150° in the horizontal and vertical directions respectively, as displayed in Fig. 4a)-b). The NDI frame with three markers was placed close to the BSFM manipulator to provide the reference frame. Another NDI marker was attached to the distal end of the BSFM manipulator for position collection. The comparison results of the experimental and kinematics-derived position values are shown in Fig. 4c)-d). The measured values are well consistent with the theoretical prediction from kinematics, and the maximum errors are 2.20mm (horizontal direction) and 1.82mm (vertical direction), accounting for 2.39% and 1.98% of the whole BSFM length. The results indicate that the BSFM manipulator features outstanding constant curvature performance and bending motions. The maximum error occurs at around the maximal bending angles due to the uneven tension distribution and increased internal friction between the vertebrae. Furthermore, the maximum bending angle was tested as 247°, which can meet the demand for bending performance for the vast majority of surgeries.

2) Accuracy Analysis of In-situ Torsional Motion

The in-situ torsional accuracy of the proposed BSFM was verified in different bending configurations, as shown in Fig. 5. In each set of tests, the initial bending angles were set to 30°, 45°, 60°, 75°, and 90°, after which the BSFM manipulator was driven to rotate 360° with the distal end direction kept constant. The NDI optical tracking unit measured the distal position

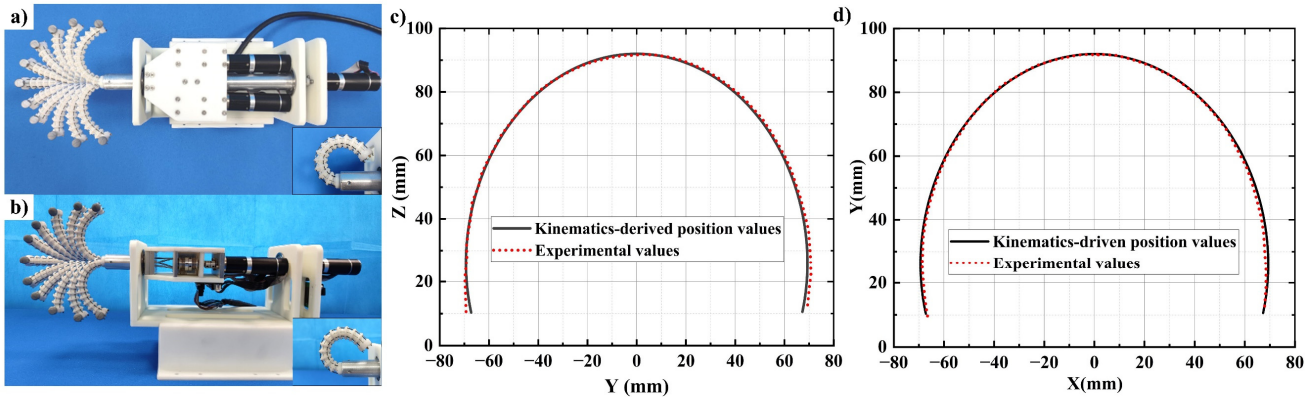

Fig. 4. Bending performance tests of the BSFM manipulator. a) Bending performance tests in the horizontal direction. b) Bending performance tests in the vertical direction. c) Comparison results of the experimental and kinematics-derived position values in the horizontal direction. d) Comparison results of the experimental and kinematics-derived position values in the vertical direction.

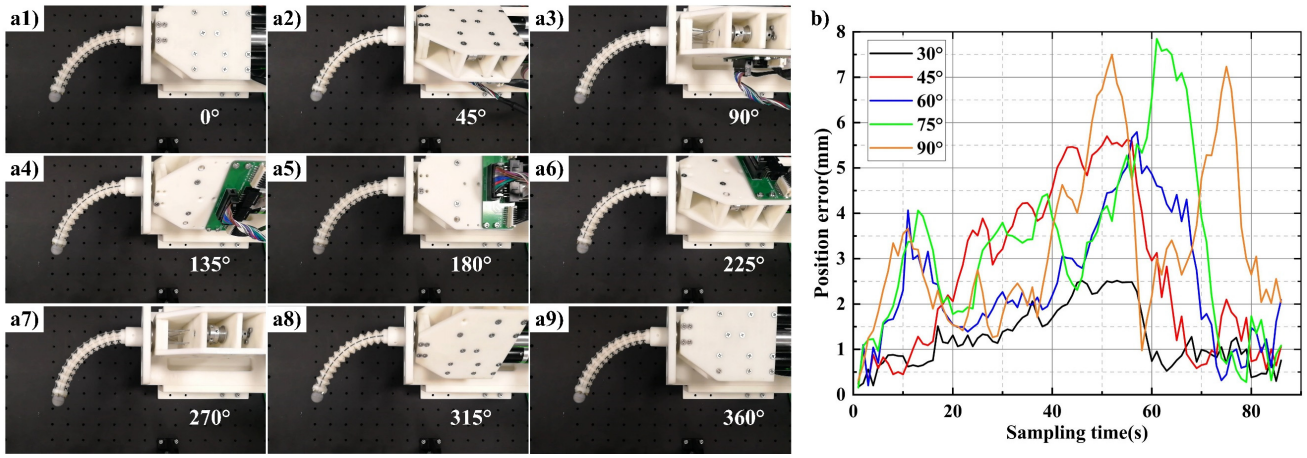

Fig. 5. In-situ torsional motion accuracy test. a) The process of the in-situ torsional motion at a bending angle of 75°. b) Position errors at different bending angles when performing in-situ torsional motion for a full circle.

TABLE II
POSITION ERRORS AT DIFFERENT BENDING ANGLES

Bending Angle [deg]	Average Error [mm]	Proportion [%]
30	1.25	1.36
45	2.66	2.89
60	2.47	2.68
75	3.22	3.50
90	3.29	3.58

errors, as shown in Fig. 5b) and Table II. It can be seen that the maximum average error is 3.29mm, accounting for 3.58% of the total length. This result indicates that the kinematic model of in-situ torsion is accurate, and the proposed BSFM manipulator supports an easy implementation for in-situ torsion motion.

C. Tests for Loading Capacity and Torsional Stiffness

1) Loading Capacity Test

To investigate the loading capacity, the standard weights were loaded at the distal end of the BSFM manipulator with an incremental step of 50g, as displayed in Fig. 6. The BSFM manipulator was configurated with different initial angles of 0°, 30°, 60°, and 90°in both horizontal (Fig. 6a)) and vertical (Fig. 6b)) directions to bear the loading of the standard weights. The optical NDI unit measured the distal deflection of the BSFM manipulator. Each set of experiments was repeated three times, and the averaged values were utilized to present the distal weight-deflection relationship, as illustrated in Fig. 6c)-d). The deflection variation is less than 10% under about 1N loading, regardless of the initial bending angle, and the loading capacity is enhanced with increasing bending angle. In addition, the manipulator can maintain a small deflection variation with a 4.5N distal load when the bending angle is 90° (9.49mm in the horizontal direction and 10.52mm in the vertical direction).

2) Torsional Stiffness Test

The torsional stiffness of the proposed flexible manipulator was experimentally investigated, as shown in Fig. 7a). Its proximal end was connected to a Maxon DC motor, and its distal end was connected to a 6-axis force/torque ATI sensor. The motor was driven to produce a torsional motion with a step size of 0.9°, and the corresponding torque values at different torsional angles were measured. Furthermore, the BSFM manipulator and the traditional SFM manipulator have been made with the same structural parameters for experimental comparison. Each set of experiments was repeated three times, and the experimental results were averaged. As shown in Fig. 7b), the measured data is linearly fitted by the least square

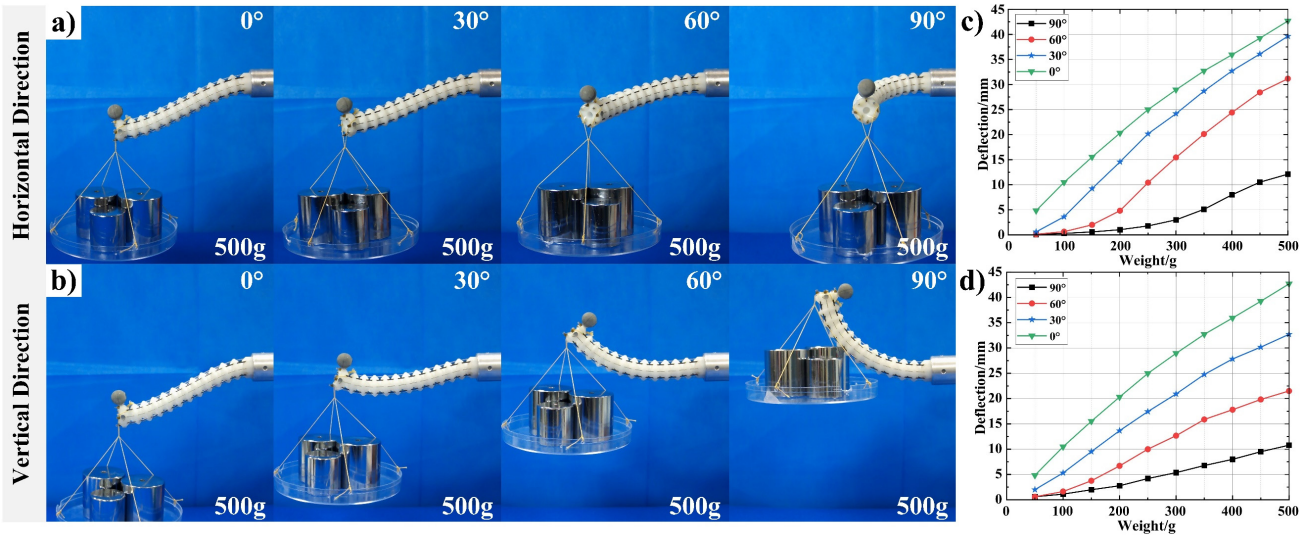

Fig. 6. Loading capacity tests for the BSFM manipulator in different bending directions. a) Loading capacity tests in the horizontal direction. b) Loading capacity tests in the vertical direction. c) Experimental results in the horizontal direction. d) Experimental results in the vertical direction.

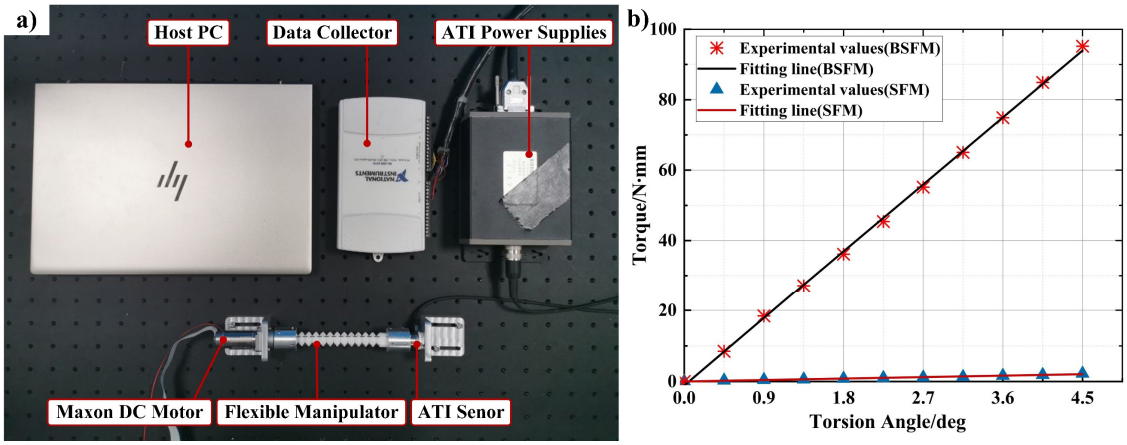

Fig. 7. Torsional stiffness tests for the BSFM and SFM manipulators. a) Experimental setup for torsion test. b) The relationship between the torque and the twisting angle.

method and the slope of the fitted line is the torsional stiffness. The calculated torsional stiffness of the BSFM manipulator is about 21.13N·mm/deg, which is 46 times higher than that of the SFM manipulator. Therefore, the proposed BSFM features excellent torsional stiffness for effective torque transfer.

D. Phantom Experiment for the Larynx

An anatomical model (HONGMO, Shanghai, China) which realistically reproduces the structure of the human mouth and larynx is utilized to verify the feasibility of the proposed BSFM in MIFS, and the experimental setup is shown in Fig. 8a). The BSFM robot was mounted onto a UR10 robot, and an endoscopic camera (WS-MM1-L09, WISERSCOPE, Guangzhou, China) was attached to the distal end of the BSFM manipulator to provide visual information. As shown in Fig. 8b), the forward movement of the endoscope was achieved by the UR robot, and the orientation of the endoscope was controlled by the deflection of the BSFM manipulator. After the endoscope reached the target lesion position, it could perform in-situ torsional motion to realize posture adjustment without changing the position, as displayed in Fig. 8c1)-c2), which expands the exploration range and facilitates the observation and operation for surgeons. This experiment proves that the design can be well applied in MIFS for laryngeal exploration.

E. Discussion

The performance comparison with other flexible manipulators is summarized in Table III. This manipulator features outstanding anti-torsion capacity with a torsional stiffness of 21.13N·mm/deg since the circumferential rotation between the vertebrae is constrained by four ball pins, which is obviously better than other flexible manipulators, and effectively improves the in-situ torsional motion accuracy with a maximum average error of 3.58%. In addition, the friction between vertebrae is significantly reduced by the point contact between the ball pins and guideways, and the gap distance between vertebrae is also minimized due to the trapezoidal spacer design, thus enabling the designed manipulator to yield a smooth bending shape with constant curvature, whose

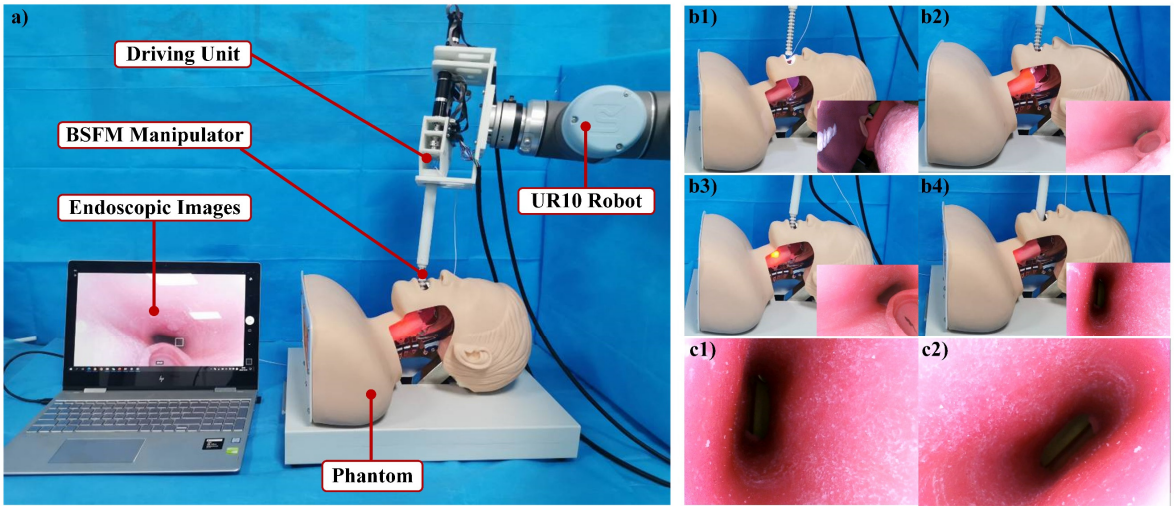

Fig. 8. Phantom experiment. a) Experimental setup for validation on a laryngeal phantom. b) Transoral access process of the proposed manipulator. c) Enlarged views of the endoscope during the in-situ rotational motion.

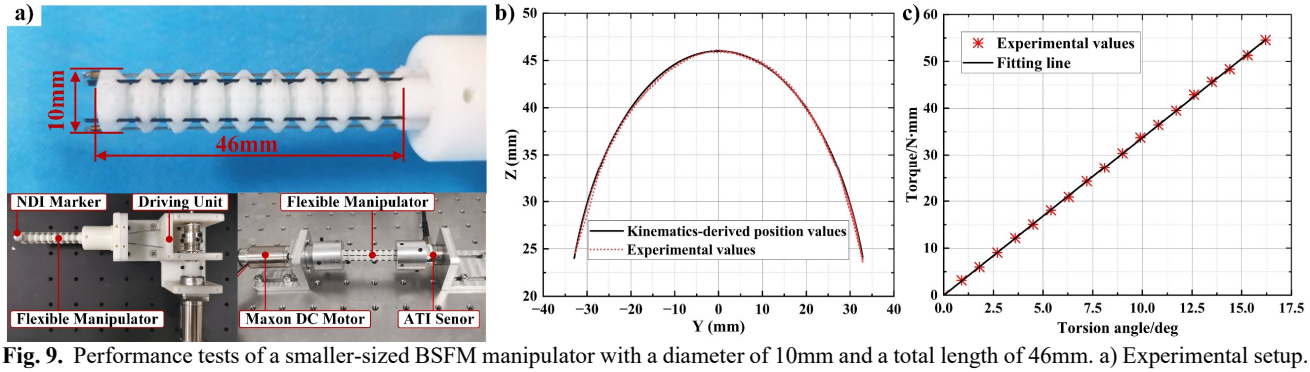

Fig. 9. Performance tests of a smaller-sized BSFM manipulator with a diameter of 10mm and a total length of 46mm. a) Experimental setup. b) Results of the bending performance test. c) Results of the torsional stiffness test.

maximum position errors are 2.39% (horizontal direction) and 1.98% (vertical direction). This method can effectively predict the distal trajectory of the BSFM manipulator under the assumption of constant bending curvature to achieve accurate motion control. The maximum payloads of the BSFM manipulator in both bending directions are both more than 4N, indicating that this design features excellent loading capacity to meet the surgical demand. Therefore, the proposed BSFM manipulator demonstrates excellent performance with a favorable trade-off between dexterity and stiffness.

Furthermore, a small-sized BSFM manipulator with a diameter of 10mm and a total length of 46mm was fabricated to further investigate and validate the performances of the proposed design. The experimental setups for performance evaluation regarding the bending motion and torsional stiffness have been configured as shown in Fig. 9a). The experimental procedures were performed with the same steps for the larger-sized BSFM manipulator. The maximum error between the experimental and kinematics-derived position values within [-90°, 90°] was 0.77mm, accounting for 1.68% of the total length, as illustrated in Fig. 9b). In addition, the results demonstrate that the torsional stiffness of this manipulator is 3.37N·mm/deg, as shown in Fig. 9c). Therefore, the design can still maintain excellent performance at small sizes. The processing accuracy of the BSFM manipulator is high and the strength of the resin material is low, which leads to wear and extrusion deformation of the vertebrae after some time, thus affecting the motion accuracy. In the future, the life of the BSFM manipulator can be improved by using metal material manufacturing. The errors of the in-situ torsional motion may originate from three aspects. Firstly, there exists hysteresis when a pair of cables are driven by a driving wheel because the required changes in cable length are different. This error can be depressed by switching to screws to drive the cables in the future. Secondly, the motors have a large tooth gap, which may reduce the control accuracy. Thirdly, the error may originate from the excessive constraint of the elastic backbone at a large bending radius. The phantom experiment demonstrates that the proposed design can be well applied in MIFS to assist surgeons.

The kinematic model of the flexible manipulator without any loading has been derived and achieves a relatively high motion accuracy in the free space. However, the performance of this kinematic model will degrade when the flexible manipulator is configured with a lengthier structure that contains more vertebrae. The complex and dynamic scenarios, such as unknown external loads, internal deformation, backlash, and time-varying friction under different cases, will also significantly contribute to this model degradation. Thus,

TABLE III
THE PERFORMANCE COMPARISON OF SEVERAL FLEXIBLE MANIPULATORS

Group	Bending range	DOFs	Maximum position error of the bending motion	Maximum average error of the in-situ torsional motion	Loading capacity	Torsional stiffness	Outer diameter
Kim et al [15]	±180°	1	4.25%	\	2.5N	\	15.9mm
Kong et al [10]	±120°	2	\	5.75%	2N	\	\
Zhang et al [9]	±60°	2	12.9%	\	\	≈1.67N·mm/° (simulated)	10mm
Li et al [28, 29]	±90°	1	\	6.10% (estimated)	2.6N	\	15mm
This work	**±150°**	**2**	**2.39%* 1.98%****	**3.58%**	**4.3N* 4.4N****	**21.13N·mm/°**	**15mm**

*In the horizontal plane; **In the vertical plane.

significantly contribute to this model degradation. Thus, complex kinematic and dynamic models need to be further investigated. Recursive algorithms support deriving the motion equations of kinematics and dynamics for serial robots by constructing several typical recursive formulations [30–32]. These algorithms can simplify complex dynamic problems and reduce computational complexity, facilitate efficient computational costs, and support the real-time implementation of inverse dynamics [31,32]. Recent advances in recursive algorithms support the derivation of motion equations for mobile robotic manipulators with viscoelastic links and revolute-prismatic flexible joints, and variable-length multi-section continuum/soft arms [33–36]. These merits support their applications for the serial chain robotic systems to automatically obtain the governing equations and address the laborious and complicated issues for kinematics and dynamics under complex scenarios, which can be further applied to the proposed flexible manipulator with a serial chain of the vertebrae in the future. The developed proximal and distal force sensor designs and fiber Bragg grating (FBG)-based shape sensing techniques in our previous work will also be further integrated with the flexible manipulator to provide force feedback and enable closed-loop control [37,38].

VI. CONCLUSION

A novel flexible manipulator based on a ball-and-socket joint has been proposed and implemented to improve the bending performance and torsional stiffness to enable excellent control accuracy and effective in-situ torsional motion for improving its dexterity and expanding its workspace. Compared with other manipulators, the presented BSFM manipulator overcomes high and uneven friction, poor anti-torsion capacity, and static instability, providing a favorable balance of dexterity and stiffness. Meanwhile, the proposed BSFM manipulator can effectively transfer torque and be applied to the in-situ torsional motion to overcome the limitation of insufficient dexterity of flexible manipulators in torsional motion, thus extending the application of the design in surgery. A series of performance validation experiments and a phantom test in the larynx have been performed to verify the performance characteristics of the designed BSFM manipulator and its potential for clinical feasibility in MIFS. Furthermore, the BSFM manipulator also provides excellent bending performance and stiffness at small sizes. Future work will further utilize force and shape sensing techniques to enable real-time shape estimation and tip localization, and integrate instruments such as flexible drills and biopsy forceps to implement applications in other narrow cavity environments.

REFERENCES

[1] M. O. Omisore, S. Han, J. Xiong, H. Li, Z. Li, and L. Wang, "A review on flexible robotic systems for minimally invasive surgery," *IEEE Trans. Syst. Man Cybern Syst*, vol. 52, no. 1, pp. 631–644, Jan 2022.

[2] V. Vitiello, S.-L. Lee, T. P. Cundy, and G. Yang, "Emerging robotic platforms for minimally invasive surgery," *IEEE Rev Biomed Eng*, vol. 6, pp. 111–126, 2013.

[3] C. Shi, X. Luo, P. Qi, T. Li, S. Song, Z. Najdovski, T. Fukuda, H. Ren, "Shape sensing techniques for continuum robots in minimally invasive surgery: A survey," *IEEE Trans. Biomed. Eng.*, vol. 64, no. 8, pp. 1665-1678, Aug. 2017.

[4] J. Zhu, L. Lyu, Y. Xu, H. Liang, X. Zhang, H. Ding, and Z. Wu, " Intelligent soft surgical robots for next‐generation minimally invasive surgery," *Advanced Intelligent Systems*, vol. 3, no. 5, pp. 2100011, May 2021.

[5] J. Burgner-Kahrs, D. C. Rucker, and H. Choset, "Continuum robots for medical applications: A survey," *IEEE Trans Robot*, vol. 31, no. 6, pp. 1261–1280, Dec 2015.

[6] J. Kim, M. de Mathelin, K. Ikuta, and D.-S. Kwon, "Advancement of flexible robot technologies for endoluminal surgeries," *Proc IEEE*, vol. 110, no. 7, pp. 909–931, Jul 2022.

[7] Y. Song, S. Wang, X. Luo, and C. Shi, "Design and optimization of a 3D printed distal flexible joint for endoscopic surgery," *IEEE Trans Med Robot Bionics*, vol. 4, no. 1, pp. 38-49, Feb, 2022.

[8] X. Luo, D. Song, Z. Zhang, S. Wang, and C. Shi, "A novel distal hybrid pneumatic/cable driven continuum joint with variable stiffness capacity for flexible gastrointestinal endoscopy," *Advanced Intelligent Systems*, no. DOI: 10.1002/aisy.202200403, 2023.

[9] X. Zhang, Y. Xian, Z. Cui, P. W. Y. Chiu, and Z. Li, "Design and modeling of a novel DNA-inspired helix-based continuum mechanism (DHCM)," *Mech. Mach. Theory*, vol. 171, p. 104702, May 2022.

[10] Y. Kong, J. Wang, N. Zhang, S. Song, and B. Li, "Dexterity analysis and motion optimization of in-situ torsionally-steerable flexible surgical robots," *IEEE Robot Autom Lett*, vol. 7, no. 3, pp. 8347–8354, Jul 2022.

[11] Y. Kong, S. Song, N. Zhang, J. Wang, and B. Li, "Design and kinematic modeling of in-situ torsionally-steerable flexible surgical robots," *IEEE Robot Autom Lett*, vol. 7, no. 2, pp. 1864–1871, Apr 2022.

[12] F. Jelínek, E. A. Arkenbout, P. W. J. Henselmans, R. Pessers, and P. Breedveld, "Classification of joints used in steerable instruments for minimally invasive surgery—A review of the state of the art," *J Med Devices*, vol. 9, no. 1, p. 010801, Mar 2015.

[13] Y.-J. Kim, S. Cheng, S. Kim, and K. Iagnemma, "A stiffness-adjustable hyper-redundant manipulator using a variable neutral-line mechanism for

minimally invasive surgery," *IEEE Trans Robot*, vol. 30, no. 2, pp. 382–395, Apr 2014.
[14] P. Berthet-Rayne, K. Leibrandt, K. Kim, C. A. Seneci, J. Shang, and G. Yang, "Rolling-joint design optimization for tendon driven snake-like surgical robots," in *2018 IEEE/RSJ International Conference on Intelligent Robots and Systems (IROS)*, pp. 4964–4971, Oct 2018.
[15] H. Kim, J. M. You, M. Hwang, K.-U. Kyung, and D.-S. Kwon, "Sigmoidal auxiliary tendon-driven mechanism reinforcing structural stiffness of hyper-redundant manipulator for endoscopic surgery," *Soft Robot*, Jun 2022.
[16] M. Hwang and D.-S. Kwon, "Strong continuum manipulator for flexible endoscopic surgery," *IEEE-ASME Trans Mechatron*, vol. 24, no. 5, pp. 2193–2203, Oct. 2019.
[17] C. Song, I. S. Mok, P. W. Chiu, and Z. Li, "A novel tele-operated flexible manipulator based on the da-Vinci research kit," in *2018 13th World Congress on Intelligent Control and Automation (WCICA)*, pp. 428–432, Jul 2018.
[18] F. Wang, H. Wang, J. Luo, X. Kang, H. Yu, H. Lu, Y. Dong, X. Jia, "FIORA: A flexible tendon-driven continuum manipulator for laparoscopic surgery," *IEEE Robot Autom Lett*, vol. 7, no. 2, pp. 1166–1173, Apr 2022.
[19] A. Gao, N. Liu, M. Shen, M. E.M.K. Abdelaziz, B. Temelkuran, and G. Yang, "Laser-profiled continuum robot with integrated tension sensing for simultaneous shape and tip force estimation," *Soft Robot.*, vol. 7, no. 4, pp. 421–443, Aug. 2020.
[20] C. J. Payne, G. Gras, M. Hughes, D. Nathwani, and G. Yang, "A hand-held flexible mechatronic device for arthroscopy," in *2015 IEEE/RSJ International Conference on Intelligent Robots and Systems (IROS)*, pp. 817–823, Sep 2015.
[21] Z. Li, H. Ren, P. W. Y. Chiu, R. Du, and H. Yu, "A novel constrained wire-driven flexible mechanism and its kinematic analysis," *Mech Mach Theory*, vol. 95, pp. 59–75, Jan. 2016.
[22] Z. Li, H. Yu, H. Ren, P. W. Y. Chiu, and R. Du, "A novel constrained tendon-driven serpentine manipulator," in *2015 IEEE/RSJ International Conference on Intelligent Robots and Systems (IROS)*, pp. 5966–5971, Sep 2015.
[23] W. Hong, L. Xie, J. Liu, Y. Sun, K. Li, and H. Wang, "Development of a novel continuum robotic system for maxillary sinus surgery," *IEEE-ASME Trans. Mechatron*, vol. 23, no. 3, pp. 1226–1237, Jun 2018.
[24] X. Dong, M. Raffles, S. Cobos-Guzman, D. Axinte, and J. Kell, "A novel continuum robot using twin-pivot compliant joints: Design, modeling, and validation," *J. Mech. Robot.*, vol. 8, no. 2, Nov 2015.
[25] J. Kim, S. Kwon, Y. Moon, and K. Kim, "Cable-movable rolling joint to expand workspace under high external load in a hyper-redundant manipulator," *IEEE-ASME Trans Mechatron*, vol. 27, no. 1, pp. 501–512, Feb 2022.
[26] Y. Hu, L. Zhang, W. Li, and G. Yang, "Design and fabrication of a 3-D printed metallic flexible joint for snake-like surgical robot," *IEEE Robot Autom Lett.*, vol. 4, no. 2, pp. 1557–1563, Apr 2019.
[27] J. Suh, K. Kim, J. Jeong, J. Lee, "Design considerations for a hyper-redundant pulleyless rolling joint with elastic fixtures," *IEEE-ASME Trans Mechatron*, vol. 20, no. 6, pp. 2841–2852, Dec. 2015.
[28] W. Li, Y.-Y. Tsai, G. Yang, and B. Lo, "A novel Eendoscope design using spiral technique for robotic-assisted endoscopy insertion," in *2020 IEEE/RSJ International Conference on Intelligent Robots and Systems (IROS)*, pp. 3119–3124, Oct. 2020.
[29] W. Li, M. Shen, A. Gao, G. Yang, and B. Lo, "Towards a snake-like flexible robot for endoscopic submucosal dissection," *IEEE Trans. Med. Robot. Bionics*, vol. 3, no. 1, pp. 257–260, Feb. 2021.
[30] J. M. Hollerbach, "A recursive Lagrangian formulation of maniputator dynamics and a comparative study of dynamics formulation complexity," *IEEE Trans. Syst. Man Cybern.-Syst.*, vol. 10, no. 11, Art. no. 11, Nov. 1980.
[31] A. Mohan and S. K. Saha, "A recursive, numerically stable, and efficient simulation algorithm for serial robots," *Multibody Syst. Dyn.*, vol. 17, no. 4, 291–319, May 2007.
[32] M.H. Korayem, A.M. Shafei, "Motion equation of nonholonomic wheeled mobile robotic manipulator with revolute–prismatic joints using recursive Gibbs–Appell formulation," *Appl. Math. model.*, vol. 39, no. 5, pp. 1701–1716, Mar. 2015.
[33] I. S. Godage, G. A. Medrano-Cerda, D. T. Branson, E. Guglielmino, and D. G. Caldwell, "Dynamics for variable length multisection continuum arms," *Int. J. Robot. Res.*, vol. 35, no. 6, pp. 695–722, May 2016.
[34] M.H. Korayem, S.F. Dehkordi, "Derivation of motion equation for mobile manipulator with viscoelastic links and revolute–prismatic flexible joints via recursive Gibbs–Appell formulations." *Robot. Auton. Syst*, vol. 103, No. 7, pp. 175-198, 2018.
[35] M.H. Korayem, S.F. Dehkordi, "Dynamic modeling of flexible cooperative mobile manipulator with revolute-prismatic joints for the purpose of moving common object with closed kinematic chain using the recursive Gibbs–Appell formulation," *Mech. Mach. Theory*, vol. 137, pp. 254-279, July 2019.
[36] C. Della Santina, C. Duriez, and D. Rus, "Model based control of soft robots: A survey of the state of the art and open challenges." *arXiv*, Oct 2021.
[37] C. Shi, D. Song, D. Lai, and S. Wang, "Development of a high-sensitivity proximal force/torque sensor based on optical sensing for intravascular robots," *IEEE Trans Med Robot Bionics,* vol. 4, no. 4, pp. 957-966, 2022.
[38] Z. Tang, S. Wang, M. Li, and C. Shi, "Development of a distal tri-axial force sensor for minimally invasive surgical palpation," *Trans. Med. Robot. Bionics*, vol. 4, no. 1, pp. 145-155, 2022.